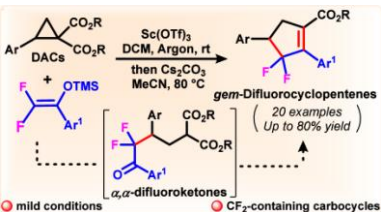
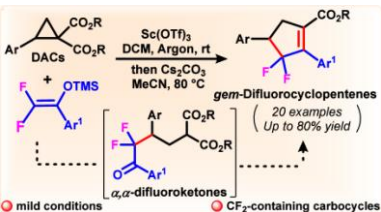
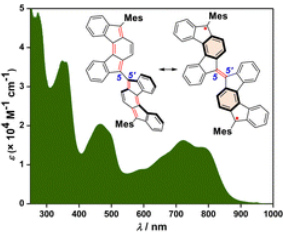
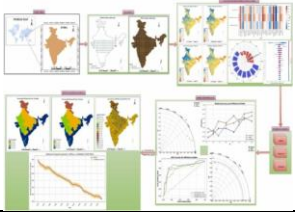


Sl. No.	<p style="text-align: center;"><b>IIT Ropar</b>  <b>List of Recent Publications with Abstract</b>  <b>Coverage: March, 2025</b></p>
A	<p style="text-align: center;"><b>Conference Proceeding(s)</b></p>
1.	<p><a href="#"><u>Agro-waste materials used for producing energy and sustainability applications: A review on waste to energy</u></a>  <b>J Kumar, P Kumar, VK Chaudhary</b> - International Conference on Recent Advancements in Mechanical Engineering, (ICRAME- 2024), 2024</p> <p><b>Abstract:</b> The development of an industrialized economy is based on energy. All human endeavors, particularly those involving space travel, water heating, food manufacturing, etc., actually depend on it. The components from agricultural waste that are utilized to produce a lot of energy and sustainability in industrial production are the basis of this review article. The agricultural waste sector has the potential to significantly worsen environmental degradation, which endangers both human and animal health. The production of bioenergy from agricultural industrial wastage, a significant source of agro crop residue, is seen as a potential technique that could help combat environmental pollution and the depletion of fossil fuels. This research paper is based on agro-waste products used in bioenergy generation and sustainability development. Some bioagro-waste fibers are used in building constructions and some straw and husk are used in biofuel production. Large-scale use of agricultural industrial wastes as raw materials also alleviates waste management issues that would otherwise accumulate and have detrimental consequences on the environment and human health. After getting the final result, the basic focus of this review is on producing bioenergy by valuing agro-industrial wastes. Additionally, it goes over the many approaches used to produce various biofuels, such as biofuel, biogas, bioethanol, biodiesel, and biohydrogen. The analysis goes on to discuss the production methods, constraints, and future potential of agricultural industrial wastes as a feedstock for waste management and the production of bioenergy. It provides a thorough understanding of the integrating polymerization and using water for hydrolysis of waste product biomass, which can be a step toward a “cleaner ecosystem and future” and efficiently utilized as a “green tool” in a variety of factories, such as biorefinery and sustainable production applications.</p>
2.	<p><a href="#"><u>BLE receiver antenna design for monitoring and sensing applications</u></a>  <b>R Raina, S Kumar</b> - International Conference on Agriculture-Centric Computation, (ICA, 2024), 2025</p> <p><b>Abstract:</b> Bluetooth stands out as the top choice among wireless technologies for low-power, short-range applications in the realm of the Internet of Things (IoT). Double inverted F antenna (DIFA) as a Bluetooth Low Energy (BLE) receiver also known as scanner is proposed in this paper for monitoring and sensing applications. The proposed DIFA enables real-time monitoring of cow health. The proposed receiver antenna continuously receives the data from the transmitting device which includes the accelerometer sensor tied on the neck of the cow and then sends the received data to the cloud, thus, can quickly identify any anomalies or signs of distress in individual cows or the entire herd. The proposed DIFA is simulated using Ansys High Frequency Structure Simulator (HFSS). It operates within the frequency range of 2.40–2.50 GHz, featuring resonant frequency of 2.45 GHz. It possesses –36.23 dB return loss, 4.08% bandwidth percentage and 1.7 dBi gain. Furthermore, comparative analysis has been conducted to assess the enhanced performance of the proposed DIFA with defected ground structure (DGS) in comparison to the DIFA without DGS. Fabrication of the proposed DIFA with DGS technique has been done on FR4 substrate with size of 106 mm × 40 mm and the measured results closely match the simulated findings. Moreover, proposed DIFA is subjected to testing in both indoor</p>

	and outdoor environments, confirming its functionality in the far field.
3.	<p><a href="#">Challenges and outcomes of organizing an open discussion forum for building the csed research community</a>  <b>N Goel, B Shah, M Kumar, R Murali, R Gupta</b> - Annual ACM India Compute Conference (COMPUTE, 2024), 2025</p> <p><b>Abstract:</b> In India, there are concerns about the learning quality and the skill set of the graduates, as only 47% are estimated to be employable. It is a large and significant problem that needs to be researched and addressed by a community of Indian CS educators and researchers (CSEd). To foster such a community, we have been running a paper-reading activity for sixteen months. This paper reports on the experience of running such an open-group research discussion forum and investigates the impact on the CSEd research community-building process. Every month, this activity begins by selecting a paper based on specific criteria and inviting interested participants to an online discussion session. Major activities during the discussion are recorded for further analysis. To understand the impact of the activity better, we also conducted a survey of community members at the end of this period. The paper shows that the primary challenge is to get unique community members to join the session; a participant who stayed for a few minutes attended the entire session. We find that the factors for keeping the discussion engaging while promoting active participation included starting the discussion with a paper briefing, the presence of domain experts, and having the paper's author present during the discussion. The survey respondents mostly agreed that the activity is important and should be continued. They also provided useful suggestions to make the sessions more effective for the participants, including making it easy for those who didn't read the paper before joining.</p>
4.	<p><a href="#">EMI reducing inverted F slot on reference plane of mixed signal design</a>  <b>LK Baghel, R Singh, S Kumar, SA Sis, L Catarinucci</b> - 2024 IEEE Asia-Pacific Microwave Conference (APMC, 2024), 2025</p> <p><b>Abstract:</b> In mixed-signal design, slots on reference planes are the most preferred choice to isolate return currents of sensitive analog and noisy digital signals. However, the discontinuity caused by these slots in the return current path leads to unwanted radiation, which causes electromagnetic interference (EMI) issues. Hence, in this context, we propose inverted F slot structure to be used in place of the conventional slot structure, which alleviates the return current path discontinuity and provides a low impedance path for return current. This, as a result, reduces unwanted radiation. The proposed inverted F structure is suitable for rigorous parametric analysis by its versatile geometry, allowing the user to tune the structure size to minimize the radiation at the desired frequency. Furthermore, the simulations of the inverted F slot structure, performed on a 70×45mm RO4003 Rogers PCB in the frequency range of 1-5GHz, show a maximum improvement of 55dB with inverted F slot and 32dB with inverted F split, which outperforms the existing solutions.</p>
5.	<p><a href="#">Investigation of thermal characteristics of biomass for energy utilization through differential scanning calorimetry</a>  <b>SA Waziri, I Dhada, R Das</b> – 10th Thermal and Fluids Engineers Conference (TFEC), 2025</p> <p><b>Abstract:</b> Eminent burdens caused by the energy deficit and environmental degradation necessitate the exploration of forestry and agricultural wastes and transform them into accessible sustainable fuels in contemporary society. This is to meet up with the rising energy demand for various critical sectors of human endeavours. In this study, the thermal decomposition and stability aspects of eight feedstocks (<i>Populus ciliata</i>, <i>Eucalyptus globulus</i>, <i>Graminae saccharum officinarum</i>, <i>Cocos nucifera</i>, <i>Panicum virgatum</i>, <i>Oryza sativa</i>, <i>Zea mays</i>, and <i>Parthenium hysterophorus</i>) found in northern India, were investigated through Differential Scanning Calorimetry (DSC). The experiments were carried out starting from 30°C to 800°C at a temperature ramping step of 15 °C/minute, held for 2 minutes at 800°C. Specific enthalpy</p>

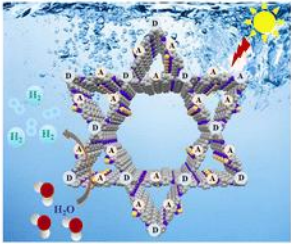
	<p>changes (endothermic) in the range of <math>11.06 \text{ J}\cdot\text{g}^{-1}</math> – <math>112.87 \text{ J}\cdot\text{g}^{-1}</math> were noted around <math>100^{\circ}\text{C}</math> which resulted from moisture removal. The breakdown of hemicellulose and cellulose resulted in endothermic peaks in the range of <math>200^{\circ}\text{C}</math> – <math>400^{\circ}\text{C}</math> in the samples. However, an exothermic process was recorded in <i>Populus ciliata</i> nearly at <math>351^{\circ}\text{C}</math> with a specific enthalpy of <math>-9.768 \text{ J}\cdot\text{g}^{-1}</math>, which can be attributed to the combustion of hemicellulose and cellulose due to the inherent energy potential of the <i>Populus ciliata</i>. DSC reveals that hemicellulose is the most unstable constituent during the thermal process, followed by cellulose and lignin. Moreover, results from this study provide significant insights into the thermochemical conversion of the studied sample biomasses with possible extension to evaluate their synergistic effect when blended.</p>
6.	<p><a href="#">Machine learning based approach to detect adulteration in turmeric using RGB and thermal images</a>  <b>R Kaur, S Singh, M Saini</b> - International Conference on Agriculture-Centric Computation, (ICA, 2024), 2025</p> <p><b>Abstract:</b> Turmeric is a widely used spice due to its medicinal, culinary, and dyeing properties. However, its frequent adulteration poses significant health risks, including heart disease, metabolic disorders, and even death. Therefore, a swift, dependable, and non-destructive method is imperative. This research paper aims to detect adulterants in turmeric using thermal and RGB images. Pure turmeric powder is blended with 20% chalk powder, chickpea powder, and starch, along with 10% tartrazine adulterants. The prepared samples undergo heating at 50 and <math>70^{\circ}\text{C}</math>, while thermal and RGB images are captured. Applying CNN and VGG16 models, we achieve accuracies of 77.11% and 63.46% on CNN, and 93.08% and 95.08% on VGG16 for thermal images at 50 and <math>70^{\circ}\text{C}</math>, respectively. For RGB, we attain accuracies of 68.18% on CNN and 95.45% on VGG16. These results indicate the viability of detecting adulteration using thermal images, with VGG16 demonstrating superior performance.</p>
7.	<p><a href="#">Socio-demographic determinants of electric vehicle purchase intention in emerging markets: Evidence from Urban Punjab, India</a>  <b>H Ahmad, TM Rahul</b> - Proceedings of the 7th International Conference of Transportation Research Group of India (CTRG 2023), Volume 2, 2025</p> <p><b>Abstract:</b> The implementation of government initiatives aimed at promoting the adoption of electric vehicles in India has encountered limited success, prompting the need for further research in this area. The present study adds to the existing scant literature by identifying the socio-demographic characteristics that impact the potential purchase decision of electric vehicles among the urban Indian population. To achieve this goal, a one-way ANOVA was conducted to identify sociodemographic variables that have significant differences in means among their various categories. Using a binary logit model, the effect of these variables was then estimated for the potential purchase of an electric vehicle by the population. The results indicate that younger people, retired people, government sector employees, people living in large families, highly educated individuals, and part-time employees are more inclined to purchase an electric vehicle than others. No significant influence of gender, income, or current vehicle ownership was found on the decision at hand. The study's findings provide valuable insights for policymakers, electric vehicle manufacturers, and marketers to target specific subpopulations and increase the efficacy of their initiatives. The identification of key socio-demographic factors in the context of electric vehicle adoption in urban India represents a significant contribution to the current literature in this field.</p>
<b>B</b>	<b>Journal Article(s)</b>
8.	<p><a href="#">(3+2) Annulation of donor–acceptor cyclopropanes with difluoroenoxysilanes: Syntheses of gem-Difluorocyclopentenenes via <math>\alpha,\alpha</math>-Difluoroketone scaffolds</a>  <b>N Yadav, P Banerjee</b> - The Journal of Organic Chemistry, 2025</p>

	<p><b>Abstract:</b> Herein, we present an acid- and base-mediated approach for ring opening of donor–acceptor cyclopropanes (DACs) followed by (3+2) annulation, yielding biologically relevant <i>gem</i>-difluorinated cyclopentenones via <math>\alpha,\alpha</math>-difluoroketone scaffolds. Fluorinated rings are essential building blocks in drug discovery and materials research. This methodology has a broad substrate scope, is scalable, and provides a practical synthetic route to obtain value-added fluorinated compounds.</p>  <p style="text-align: center;">  </p>
9.	<p><a href="#">5,5'-Biindeno[2,1-c]fluorene: importance of C5-C5' linkage for an indeno[2,1-c]fluorene dimer exhibiting an open-shell ground state</a>  <b>N Maurya, P Jana, H Sharma, S Bandyopadhyay, S Das</b> - Chemical Communications, 2025</p> <p><b>Abstract:</b> Mesityl-protected indeno[2,1-c]fluorene and its C2–C2'-linked dimer 2,2'-biindeno[2,1-c]fluorene are closed-shell molecules. Herein, we report the synthesis and characterization of a mesityl-protected 5,5'-biindeno[2,1-c]fluorene displaying 26.4% diradical and 0.9% tetraradical characters. The C5–C5' linkage between two [2,1-c]IFs is crucial for its open-shell character, resulting in its far-red UV-vis absorption, redox amphotericism, partially <i>para</i>-quinoidal <i>as</i>-indacene core, and temperature-dependent EPR response due to a small singlet–triplet energy gap.</p> 
10.	<p><a href="#">A concurrent multi-scale framework for performance assessment of moment resisting reinforced concrete frame</a>  <b>O Mishra, ANR Chowdhury, P Haldar</b> - Engineering Structures, 2025</p> <p><b>Abstract:</b> High-fidelity (3D) finite element framework can capture the various structural damages occurring in an RC frame structure during extreme seismic events, obviating the necessity for extensive calibration. However, they are computationally intensive. Hence, the concurrent multi-scale framework can be employed as a substitute. This study proposes a concurrent multi-scale model for Reinforced Concrete (RC) structures, implemented in a nonlinear finite element analysis to investigate the governing failure mechanism. The experimental results available for RC beam-column connection are used to validate the proposed multi-scale model. Additionally, high-fidelity nonlinear finite element analyses are carried out on RC structure at the component as well as global level, and the results are used to examine the computational performance of the concurrent multi-scale framework. Afterwards, nonlinear pushover analysis and vulnerability assessment are conducted on a three-story RC frame structure to understand its seismic performance. The obtained results show that the multi-scale framework is computationally efficient and can accurately predict the seismic behaviour of RC structures.</p>
11.	<p><a href="#">A novel hybrid machine learning framework for spatio-temporal analysis of reference evapotranspiration in India</a>  <b>D Banerjee, S Ganguly, WP Tsai</b> - Journal of Hydrology: Regional Studies, 2025</p>

	<p><b>Abstract:</b> Study region: The study focuses on the diverse climatic regions of India, spanning arid, semi-arid, sub-humid, and humid zones. Study focus: This research employs a novel hybrid machine learning (ML) framework for precise spatio-temporal reference evapotranspiration (ET<sub>o</sub>) modelling from 1970 to 2024, addressing the variability in temperature, humidity, and precipitation. Three advanced ML models—Quantile-Adjusted xLSTM Network (QAxLNet), Quantile-Score Diffusion Model (QSDM), and Attentive Deep Quantile-Aware Autoencoder Network (ADAQNet)—are proposed and applied, focusing on relative humidity and temperature as critical predictors. Model validation, conducted with EEFlux-derived ET<sub>o</sub> data and Indian Meteorological Department (IMD) benchmarks, revealed strong alignment across diverse climatic zones. New hydrological insights for the region: The MPI-ESM1-2-HR model under SSP3-7.0 scenarios outperformed other CMIP6 models, with a correlation coefficient of 0.975 and spatial error of 3.55 mm. The ADAQNet demonstrated superior performance, with lowest errors RMSE (Train: 0.2247, Test: 0.2499), and R<sup>2</sup> (Train: 0.96; Test: 0.9571) among the models. ET<sub>o</sub> declined at an average rate of 1.9 mm/year, indicating the role of climate change. ET<sub>o</sub> variability closely mirrored the spatial distribution of the National Building Code (NBC) of India. Seasonal variations were significant, with arid regions (Rajasthan, Gujarat) experiencing the highest increase (2.5–5.1 mm/year). Humid regions showed high sensitivity to RH forecasts, with up to 20 % ET<sub>o</sub> deviation. The study emphasizes the spatial, temporal, and seasonal variations of ET<sub>o</sub> across the region, highlighting its dependence on climatic factors.</p> 
12.	<p><a href="#">A replay-attack-resilient power system state estimation scheme</a>  <b>S De, R Sodhi</b> - IEEE Transactions on Automation Science and Engineering, 2025</p> <p><b>Abstract:</b> Replaying outdated or uncorrelated data can lead to a distorted view of the actual system state, resulting in suboptimal control decisions that potentially compromise grid stability, reliability, and efficiency. Replay Attacks (RA) are a kind of stealthy attacks which can mar one of the very key application of the Energy Management System (EMS), viz., Power System State Estimation (PSSE). This paper, therefore, proposes a novel scheme to make the PSSE resilient against RAs. To this end, first, a Power Transfer Distribution Factor (PTDF)-assisted vulnerability analysis is carried out to identify the critical SCADA measurements which may become a preferred choice of the attacker to launch RAs. Next, an optimal number of secured phasor measurements are exploited to detect and correct any RA in the SCADA measurement set, followed by a simple hybrid estimation scheme to reconstruct the falsified set of measurements. The proposed strategy's effectiveness is validated through testing on three standard IEEE test systems, namely IEEE 14, New England (NE) 39, and IEEE 118 using simulated data generated from Real-time Digital Simulators (RTDS) and MATPOWER. Finally, the efficacy, feasibility and robustness of the proposed method under different variant of RA scenarios are compared with two existing Kalman Filter-based distributed state estimation methods associated with the three widely used statistical cyber attack detectors.</p>
13.	<p><a href="#">Ag(I)-catalyzed intramolecular cascade cyclization to construct [6-5-7-6] heterotetracyclic (-N and -O) indole fused scaffolds</a>  <b>M Kumar, A Kumar, S Devi, A Goswami</b> - Advanced Synthesis &amp; Catalysis, 2025</p> <p><b>Abstract:</b> Herein, we report a silver-catalyzed intramolecular cascade reaction of 2-alkynylaniline tethered heteroenone systems to achieve the synthesis of [6-5-7-6] heterotetracyclic indole fused benzoxepino- and benzoazepino scaffolds. The reaction proceeded through a silver(I)-initiation cascade intramolecular 5-endo-dig cyclization followed by 7-exo-</p>



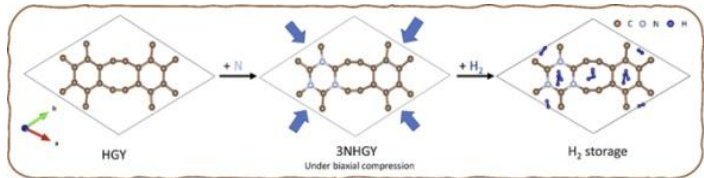
	<p>trig cyclization to enable the structurally diverse [6–5–7–6] heterotetracyclic adducts in modest to good yields.</p>
14.	<p><a href="#">Analysis of the maximum achievable throughput of extended advertisements in BLE</a>  <b>S Gautam, S Kumar</b> - IEEE Internet of Things Journal, 2025</p> <p><b>Abstract:</b> Bluetooth Low Energy (BLE) allows connectionless data transfer to take place through advertisements. Bluetooth Core Specification version 5.0 introduced extended advertising which allows each secondary channel advertising packet to carry up to 255 bytes of payload. Up to 1,650 bytes of data can be advertised as a single transmission through chaining of multiple packets carrying fragments of advertising data. This paper derives throughput expression in the presence of bit errors and analyses the maximum throughput for connectionless data transfer using extended advertisements, for all the Uncoded and Coded PHYs that offer different data rate and range capabilities. Guidelines are provided for the choice of appropriate PHYs based on the transmission size, throughput, and range requirement of the application. Simulation results have been presented that verify the analytically obtained throughput values. Since connectionless mode of communication does not allow acknowledgements from the receiver, it is essential to overcome the impact of bit errors through re-transmission of each packet for increased chances of its reception. Analysis of maximum achievable throughput with re-transmission of each data packet has also been presented in this paper. Results suggest that the maximum achievable throughput is impacted by the duration of each transmission, due to which beyond a certain value of the data size, the Low Energy (LE) Coded PHYs are unable to offer significant improvement in the amount of data delivered per unit time.</p>
15.	<p><a href="#">Assessment of solar and desiccant-assisted building air-conditioning systems for net-zero status in hot-humid conditions</a>  <b>G Singh, R Das</b> - Heat Transfer Engineering, 2025</p> <p><b>Abstract:</b> Rising consumption of traditional air-conditioning systems necessitates fossil-based electrical energy by sacrificing environmental sustainability. It thus becomes imperative to detect scopes of reducing electrical grid-based energy derived from fossil fuels, and endeavor toward promoting strategies based on clean energy sources. Hot-humid weather offers toughest challenge toward air-conditioning system design. In this paper, the operational decoupled cooling and ventilation strategies of a desiccant-integrated and solar energy-regenerated air conditioning system are assessed, when the system's dedicated outside air system (DOAS) is provided with an evaporative cooling unit, direct expansion (DX) cooling coil and an enthalpy recovery wheel (ERW). The study also assesses the suitability of utilizing DX coil condenser waste heat in desiccant-based air-conditioning systems. The study highlights the benefits of utilizing heat recovery from the indoor space in the desiccant air cooling systems, and quantifies performance indices with other commonly practiced methods such as DX coil and evaporative cooling. In particular, thermal conditions, yearly electrical energy demand patterns, solar fraction, part load ratio, predicted mean vote, predicted percentage of dissatisfied occupants and allied indices are studied. Appropriate validations are done with the available standards. The attained indoor temperature is found to be approximately within 21 °C–25 °C, whereas, the relative humidity was attained between 52-60%. This study portrays notable guidelines for implementing different modifications in the air path of desiccant-assisted DOAS. Interestingly, even with reduced cooling load of more than 25% with respect to cooling coil DOAS, ERW-aided unit offers excellent solar fraction, without significantly compromising the thermal comfort. Results eventually show that using ERW along air path of desiccant-assisted DOAS may save primary energy between 7.5 to 20.9% compared to evaporative cooling and cooling coil-assisted DOAS, respectively. Finally, an attempt has been made to realize net-zero status of the considered building by solar photovoltaic that indicated about 60.2% fulfillment of the set objective. The ERW-assisted case promotes more dehumidification of the desiccant wheel enhancing the energy savings and fulfilling the net zero target to a larger extent as compared with other cases.</p>

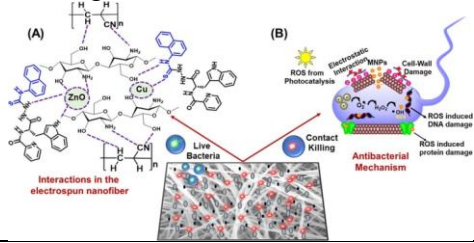
16.	<p><a href="#">Benzothiadiazole-based donor-acceptor covalent organic framework for photocatalytic hydrogen generation</a>  <b>A Nagar, G Singh, A Alam, P Pachfule, CM Nagaraja</b> - Sustainable Energy &amp; Fuels, 2025</p> <p><b>Abstract:</b> Visible light-driven water splitting to produce hydrogen (H<sub>2</sub>) is a promising strategy for harnessing renewable solar energy for the sustainable production of green fuel. Consequently, the design of materials with optimal absorption of sunlight/visible light is therefore of great importance. In this context, covalent organic frameworks (COFs), designed by rational selection of organic building blocks, represent promising semiconducting materials for photocatalytic hydrogen generation, offering a potential alternative to achieve efficient water splitting for H<sub>2</sub> generation. Herein, we demonstrate the use of a donor-acceptor COF (ETTA-BT) with benzothiadiazole (BT) moieties as the strong electron acceptor for efficient photocatalytic hydrogen generation. Interestingly, under visible light irradiation (<math>\lambda \geq 420</math> nm), the ETTA-BT COF exhibited superior photocatalytic performance with an H<sub>2</sub> generation rate of 890 <math>\mu\text{mol g}^{-1} \text{h}^{-1}</math>, which is very high as compared to ETTA-TP COF without such a donor-acceptor system. The improved catalytic performance of ETTA-BT over ETTA-TP COF has been attributed to the donor-acceptor phenomenon, which facilitates improved charge separation and migration through the “push-pull” effect. This work represents a demonstration of the application of a donor-acceptor COF for efficient and sustainable photocatalytic H<sub>2</sub> generation.</p> 
17.	<p><a href="#">BLE-driven power-efficient integrated sensing and communication framework for livestock monitoring</a>  <b>LK Baghel, R Raina, S Kumar, R Colella, L Catarinucci</b> - IEEE Journal of Radio Frequency Identification, 2025</p> <p><b>Abstract:</b> The existing BLE-based cattle health and activity monitoring solutions rely primarily on parametric power optimization. However, a cattle health and activity monitoring system may require non-optimized parameters. Further, existing solutions transmit raw data, which is usually generated frequently, consequently increasing total transmission and causing high power consumption. Besides, BLE-based solutions are prone to data loss as the number of devices in the network increases, necessitating multiple transmissions to overcome data loss. However, the lack of an analytical framework to determine the optimal number of retransmissions results in redundant transmissions. This highlights the need for analytical expressions to precisely calculate the required number of retransmissions to overcome data loss. Owing to this issue and the emergence of BLE-related solutions, we have first examined the root cause of higher power consumption. Secondly, to reduce the number of transmissions causing major power consumption, we have proposed a threshold mode that reduces the total number of transmissions and saves a significant amount of power by only transmitting parametric data over raw data, which is usually sensed and transmitted very frequently. Thirdly, we have derived analytical close-form expression for the average number of transmissions required for successful data reception, which was the critical bottleneck in existing works. As a result, we have achieved significant improvement in battery life over the existing works; in particular, we achieved a maximum battery life of 10 years in mode A (raw data transmission) and 21 years in mode B (thresholding mode).</p>
18.	<p><a href="#">Cattle verification with YOLO and cross-attention encoder-based pairwise triplet loss</a></p>

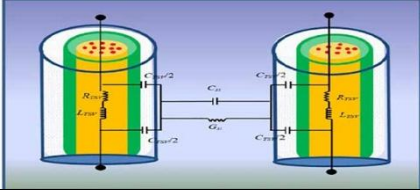
	<p>N Kumar, A Sharma, A Kumar, R Singh, SK Singh - Computers and Electronics in Agriculture, 2025</p> <p><b>Abstract:</b> Cattle identification through biometrics has increasingly relied on non-invasive methods, where facial and muzzle images are commonly used. While facial images alone offer valuable features, they can be sensitive to variations in lighting, pose, and occlusion, leading to inconsistent results. Similarly, relying solely on muzzle images, though distinct, may not provide sufficient discriminatory power for accurate identification in all cases. Combining both facial and muzzle features offers a more comprehensive solution, overcoming the limitations of using either feature independently. Recent advancements in deep neural networks have significantly influenced this field, but achieving an optimal balance between model accuracy and computational efficiency remains a challenge. In this paper, we present a novel approach by introducing a Cross-Attention Encoder in combination with a Pairwise Triplet Loss function for cattle verification. This method processes face and muzzle images in parallel, enhancing the integration of features from both inputs. The cross-attention mechanism enables the model to focus on the most relevant regions, improving feature alignment and discrimination. With a compact architecture of only 0.6 million parameters, the encoder effectively captures essential features from both the face and muzzle, ensuring precise cattle verification without excessive computational demands. Our approach achieved a testing accuracy of 93.67%, with an average inference time of 35ms per sample, demonstrating the model's efficiency. These findings highlight the strength of our attention-based method in delivering high accuracy and computational performance for cattle verification tasks.</p>
19.	<p><a href="#">Competition between the neutron-proton pair break-ups delineating the level structure of <sup>202</sup>Po</a> S Singh, D Choudhury, B Maheshwari, R Roy, K Yadav... - Physical Review C, 2025</p> <p><b>Abstract:</b> High-spin spectroscopic study of <sup>202</sup>Po (Z=84, N=118) has been carried out using the <sup>195</sup>Pt(<sup>12</sup>C,5n)<sup>202</sup>Po fusion-evaporation reaction. An extended level scheme has been proposed up to an excitation energy of <math>E_x \approx 8</math> MeV and angular momentum of <math>27\frac{1}{2}\hbar</math>, with the addition of 57 newly observed <math>\gamma</math>-ray transitions, along with the revisions in the placement of eight already known transitions and the multipolarities of four of these transitions. The energy of the unobserved <math>8^+ \rightarrow 6^+</math> transition has been proposed to be 9.0(5) keV, which resolves the uncertainty in the excitation energy of the levels above the <math>6^+</math> state. Three new sequences of <math>M1</math> transitions have also been identified in the high excitation energy regime and included in the proposed level scheme. The large-scale shell-model calculations for <math>Z &gt; 82</math> and <math>N &lt; 126</math> valence space have been carried out using PBPOP interaction, which explained the overall level scheme for both the positive and negative parity states. The calculations successfully reproduced the purity of the proton <math>\pi\frac{9}{2}</math> dominated <math>8^+</math> isomeric state, and also explained the missing <math>E2</math> decay of the <math>12^+</math> isomeric state in terms of changing nucleonic configurations.</p>
20.	<p><a href="#">Correlation of Dirac ordering with optical activity in AlB<sub>2</sub>-type Dirac MBenes</a> A Sharma - Journal of Physics: Condensed Matter, 2025</p> <p><b>Abstract:</b> Using first-principles calculations, this study systematically investigates the electronic properties and optical activity of AlB<sub>2</sub>-type Dirac MBenes alongwith their correlations. Insights from phonon-spectral calculations and <i>ab-initio</i> molecular dynamics simulations substantiates the thermally and dynamically stable character of Dirac MBenes. Electronic dispersions reveals that all Dirac MBenes exhibits finitely gapped Dirac cones (DCs) at the fermi level, while FeB<sub>2</sub> MBene behaves as a zero-band-gap semimetal akin to graphene. Such gap in DCs is desirable and crucial for optoelectronic applications. The interplay of out-of-plane <math>dxz</math> and <math>dyz</math> orbitals of metal atom and hybrids in-plane <math>dxy</math> and <math>dx^2-y^2</math> orbitals from metal atom with p orbitals from boron atoms can be attributed to the emergence of DCs in</p>



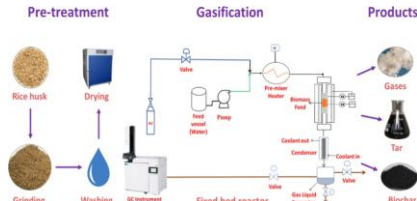
	<p>MBenes. The calculations clearly reveal that the static dielectric constant and the energy gap within the DCs are critical factors influencing the electron–hole screening effect, consequently effecting the exciton binding energy. Further, it has been demonstrated that the exciton binding energies are consistent with predictions made by the two-dimensional (2D) Mott–Wannier model, confirming the Mott–Wannier characteristics of excitons in AlB<sub>2</sub>-type Dirac MBenes, with the exception of partial Frenkel character in FeB<sub>2</sub> MBene. Furthermore, it is demonstrated that Dirac MBenes exhibit a significant light absorption capacity in the near-infrared (NIR) and visible regions, with electron–hole interactions slightly modifying the optical spectral profile, making them promising for optoelectronic and photovoltaic applications. Subsequently, covariance analysis indicates that moderate energy gaps and high static dielectric constants are conducive to hosting Mott–Wannier excitons. Additionally, careful control of d-state valence electrons and hole doping can regulate the Mott–Wannier and Frenkel character of excitons in 2D Dirac materials. Thus, this comprehensive and systematic analysis of the electronic properties and optical-excitonic behavior of AlB<sub>2</sub>-type Dirac MBenes, alongwith their correlations, enhances our understanding of this emerging family of 2D materials.</p>
21.	<p><a href="#">Design of donor–acceptor covalent organic frameworks for photocatalytic hydrogen generation</a>  <b>A Nagar, G Singh, A Alam, P Pachfule, CM Nagaraja</b> - <i>Materials Chemistry Frontiers</i>, 2025</p> <p><b>Abstract:</b> The well-ordered p-conjugated backbone facilitates efficient light absorption, enhancing carrier mobility, while the tensile molecular structure allows precise tailoring of optoelectronic properties. In addition, the alternating arrangement of donor (D) and acceptor (A) segments in the well-ordered p-conjugated framework provides pathways and channels for intermolecular charge transfer (ICT). Therefore, the precise integration of the D and A moieties into the long-range ordered backbone of the COFs accelerates carrier mobilities and reduces the possibility of electron–hole recombination. COFs with a D–A system have made great progress in the related research of photocatalytic applications. It is anticipated that COFs consisting of polar hydrophilic electron-withdrawing groups (e.g., COOH) can promote the efficient migration of photogenerated electrons to the Pt cocatalyst for the reduction of water protons to produce hydrogen. Herein, we demonstrate the tuning of hydrogen evolution activity by tailoring the functionality of pyrene-based COFs by introducing donor (D) and acceptor (A) functionalities to facilitate the effective charge separation through the push–pull effect. Further, in order to systematically study the photocatalytic performances, a series of D–A COFs with different linkages and electron-donating/withdrawing groups have been synthesized. This difference in photocatalytic hydrogen generation activity is further supported by different optical and electrochemical studies. This work highlights the rational tuning of the hydrogen generation activity of COFs by strategic incorporation of appropriate functionality.</p>
22.	<p><a href="#">Direct and indirect effect of anger and cognitive failures on subjective well-being: Mediating role of psychological distress</a>  <b>S Kharwar, P Singh</b> - <i>Psychological Studies</i>, 2025</p> <p><b>Abstract:</b> Despite the apparent significance of anger and cognitive failures (CF) in shaping Subjective Well-being (SWB), surprisingly, only some studies have investigated the nature of relationships between these variables. This study aims to investigate the direct and indirect effects of predictors anger (state &amp; trait anger) (SA &amp; SA) and CF on SWB through mediator, psychological distress (PD). SWB was operationalized as cognitive and affective evaluations and these components were measured through Satisfaction with life scale and PANAS, respectively. Employing a cross-sectional design with multi-level cluster sampling technique, 600 young adults aged 18–40 years (<math>M = 22.13</math>, <math>SD = 4.06</math>) from Uttar Pradesh, India, were assessed for relevant variables in classroom setting. The findings assert that predictors were positively associated with PD and negatively with SWB, whereas PD was negatively associated with SWB. Preacher and Hayes' (2004) mediation analysis indicates that the SA's standardized direct (<math>\beta = -0.17</math>; <math>p &lt; 0.005</math>) and indirect effect (Via PD) (<math>\beta = -0.26</math>; <math>p &lt; 0.05</math>) were significant; thus, PD</p>

	<p>partially mediated between SA and SWB. Whereas a full-mediation of PD existed between TA and SWB with a significant standardized indirect effect (<math>\beta = -0.34, p &lt; 0.01</math>), similarly, full-mediation of PD existed between CF and SWB with a significant indirect effect of PD (<math>\beta = -0.43, p &lt; 0.01</math>). The predictors emerged as substantial risk factors for SWB, especially when exacerbated by PD. Interventions with a component of emotion regulation and distress management may reduce the detrimental impacts of anger and CF by reducing the induced distress.</p>
23.	<p><a href="#">Effect of N-doping and biaxial compressive strain on H<sub>2</sub> adsorption of 2D holey graphyne monolayer via first-principles study</a>  <b>P Beniwal, B Chakraborty, TJ Dhilip Kumar</b> - International Journal of Hydrogen Energy, 2025</p> <p><b>Abstract:</b> Developing advanced materials plays an essential role in improving the efficiency and stability of hydrogen storage systems. We have explored the hydrogen storage properties of a recently synthesized holey graphyne (HGY) monolayer, considering the impacts of nitrogen doping followed by biaxial compressive strain. H<sub>2</sub> adsorption energy on the pristine HGY is too low, i.e., <math>-0.157</math> eV for a single H<sub>2</sub> adsorption, to comply with the standards for hydrogen storage. N-doping leads to improved interaction with H<sub>2</sub>, thereby the increased adsorption energy. Doping induces substantial changes in the electronic properties, as with 1 N (4.16 at.%) doping within a unit cell comprising 24 C atoms, the semiconducting nature of HGY transforms to metallic and with 6 N (25 at.%) doping, it reverts to semiconductor state featuring a reduced band gap of 0.40 eV. 3NHGY (12.5 at.% doping) is taken as the optimum case with symmetric doping and metallic nature. It shows a comparatively higher adsorption energy for a single H<sub>2</sub> molecule (<math>-0.175</math> eV). Afterward, we explored the adsorption properties of 3NHGY subjected to biaxial compressive strain. The application of compressive strain induces an increase in the electronic density in the bonds, thereby facilitating a stronger adsorption of H<sub>2</sub> molecules and thus elevating the adsorption energy. Under 4% strain, 3NHGY can adsorb 10 H<sub>2</sub> molecules with the adsorption energy within <math>-0.191</math> to <math>-0.338</math> eV, reflecting a gravimetric density of 6.42 wt%. Ab initio molecular dynamics simulation affirms the structural and thermal stability of the unstrained and strained 3NHGY monolayers. From the findings, we can infer that this study emphasizes the quest to enhance the hydrogen storage efficiency of 2D materials.</p> 
24.	<p><a href="#">Electro-elastic instability and turbulence in electro-osmotic flows of viscoelastic fluids: Current status and future directions</a>  <b>C Sasmal</b> - Micromachines, 2025</p> <p><b>Abstract:</b> The addition of even minute amounts of solid polymers, measured in parts per million (ppm), into a simple Newtonian fluid like water significantly alters the flow behavior of the resulting polymer solutions due to the introduction of fluid viscoelasticity. This viscoelastic behavior, which arises due to the stretching and relaxation phenomena of polymer molecules, leads to complex flow dynamics that are starkly different from those seen in simple Newtonian fluids under the same conditions. In addition to polymer solutions, many other fluids, routinely used in various industries and our daily lives, exhibit viscoelastic properties, including emulsions; foams; suspensions; biological fluids such as blood, saliva, and cerebrospinal fluid; and suspensions of biomolecules like DNA and proteins. In various microfluidic platforms, these viscoelastic fluids are often transported using electro-osmotic flows (EOFs), where an electric field is applied to control fluid movement. This method provides more precise and accurate flow control compared to pressure-driven techniques. However, several experimental and numerical</p>

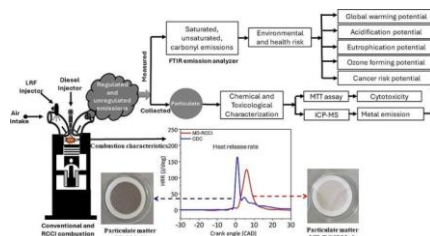
	<p>studies have shown that when either the applied electric field strength or the fluid elasticity exceeds a critical threshold, the flow in these viscoelastic fluids becomes unstable and asymmetric due to the development of electro-elastic instability (EEI). These instabilities are driven by the normal elastic stresses in viscoelastic fluids and are not observed in Newtonian fluids under the same conditions, where the flow remains steady and symmetric. As the electric field strength or fluid elasticity is further increased, these instabilities can transition into a more chaotic and turbulent-like flow state, referred to as electro-elastic turbulence (EET). This article comprehensively reviews the existing literature on these EEI and EET phenomena, summarizing key findings from both experimental and numerical studies. Additionally, this article presents a detailed discussion of future research directions, emphasizing the need for further investigations to fully understand and harness the potential of EEI and EET in various practical applications, particularly in microscale flow systems where better flow control and increased transport rates are essential.</p>
25.	<p><a href="#">Electrospun nanofibers with antibacterial and antioxidant activities for air purification</a>  <b>R Devi, M Kumar...N Singh - ACS Applied Nano Materials, 2025</b></p> <p><b>Abstract:</b> The demand for air filtration products has surged as air pollution worsens daily, particularly during the pandemic wave. Traditional air filters frequently require replacement because of the rapid dispersion of electrostatic charge and the buildup of harmful microorganisms. According to the World Health Organization, the majority of deaths related to air pollution are caused by noncommunicable diseases. To tackle these challenges, we have performed a centrifugal spinning experiment under controlled conditions, maintaining a temperature of <math>21 \pm 5</math> °C and humidity below <math>36 \pm 5\%</math>, with the nozzle positioned 10 cm from the collector. Nanofibrous membranes PZCR and PCCR were fabricated using an electrospinning method that offers strong antibacterial properties, effective air filtration, and the ability to be reused. These membranes consist of PAN nanofibers doped with ZnO and Cu nanoparticles and coated with a chitosan solution containing the antibacterial compound. Further, characterization was done by using FESEM, AFM, FTIR, and EDX spectroscopy. The average diameter of the PAN nanofiber before doping was 153 to 184 nm, and after doping, ZnO and Cu NPs were <math>225 \pm 5</math> nm and <math>455 \pm 5</math> nm, respectively. There is nearly no impact on the filtering efficiency and percentage of air resistance of the nanofiber mats, even after being treated with isopropyl alcohol, confirming compliance with ISO 16890. The membranes demonstrated a 99.9% bactericidal rate against <i>Escherichia coli</i> and <i>Staphylococcus aureus</i> bacteria, as confirmed by the ruptured bacterial cell membranes. The significant surface area relative to their volume, customizable porous structure, and ease of preparation, electrospun nanofibers make the material an ideal candidate for filtration materials, attracting significant interest in air filtration applications. Furthermore, the straining potential of these sheets remains nearly at the initial level after simple washing, outperforming commercial-grade filters.</p> 
26.	<p><a href="#">Essential frequency analysis for stacked Cu-CNT composite cells of TSVs</a>  <b>MG Kumar, Y Agrawal, P Harish, R Sharma - IEEE Access, 2025</b></p> <p><b>Abstract:</b> This paper presents a comprehensive frequency analysis of copper-carbon nanotube (Cu-CNT) composite cells in stacked through-silicon vias (TSVs), focusing on a novel approach in which Cu-CNT composite cells are distributed normally within the TSVs. This distribution is designed to simulate real-world conditions and enhance the reliability of the findings. The key</p>

	<p>contributions of this work encompass a comprehensive assessment of insertion and return losses related to electrical characteristics of stacked Cu-CNT TSVs, varying critical factors such as frequency and material composition to evaluate the system performance. Also the eye diagrams are investigated at various data rates, which shed light on the signal quality and integrity for high-speed applications. The findings show that Cu-CNT composites outperform conventional copper-based TSVs in terms of performance metrics, drawing attention to their promise as next-generation, high-density interconnects for 3D integrated circuits.</p> 
27.	<p><a href="#">Estimation of shear correction factors for laminated composite plates using variational asymptotic method</a>  <b>AK Pathak, SS Padhee</b> - Mechanics Based Design of Structures and Machines, 2025</p> <p><b>Abstract:</b> This work presents a novel method for efficiently and accurately computing shear correction factors (SCFs) in laminated composite plates. The present approach utilizes the variational asymptotic method (VAM) to derive a reduced-order plate model, providing analytical expressions for transverse shear strains in terms of 2D variables (functions of in-plane coordinates only). By matching the transverse shear forces and strain energies from VAM to those from the classical first-order shear deformation theory (FSDT) with SCFs, we extract the SCFs without cumbersome numerical evaluations. This method offers several advantages over traditional techniques: it is asymptotically accurate, computationally efficient, and provides insights into the influence of individual lamina thickness and lay-up sequence on SCFs. The presented approach can be extended to analyze the impact of other parameters such as boundary conditions and loading opening a scope for future investigations.</p>
28.	<p><a href="#">Experimental investigation of process parameters for hydrogen-rich syngas production from rice husk gasification</a>  <b>A Kumar, DS Pandey, T Mondal</b> - Sustainable Chemistry for Climate Action, 2025</p> <p><b>Abstract:</b> The overconsumption of conventional fossil fuel by the energy and petrochemical sectors demands for the development of alternate renewable sources. Biomass is found to be an effective alternate renewable energy source for the carbon-neutral production of energy and chemicals. Rice husk, one of the most common and abundant lignocellulosic biomass in Asia, is used in the present work as potential feedstock for the thermochemical conversion through gasification process in a lab-scale fixed bed (downdraft) reactor. In this work, the influence of various parameters such as the physico-chemical properties of the biomass, the temperature of gasifier, the size of the particles, the steam flow rate, equivalence ratio (ER) and gasifying agents such as mixture of (air + steam) and steam alone were investigated. The (air + steam) mixture at an ER of 0.27, steam flow rate of <math>0.775 \text{ ml.min}^{-1}</math>, and the reactor temperature at <math>950^\circ\text{C}</math>, yielded the highest hydrogen of <math>\sim 40\%</math> (vol.) and carbon monoxide of <math>\sim 12\%</math> (vol.) with a high heating value (HHV) of <math>\sim 7 \text{ MJ.m}^{-3}</math>. In contrast, when the experiments were conducted using steam alone as the gasifying agent at an ER of 0.24 with steam flow rate <math>0.6 \text{ ml.min}^{-1}</math> and the reactor temperature <math>950^\circ\text{C}</math>, the produced syngas reported to have a HHV of <math>\sim 11 \text{ MJ.m}^{-3}</math> with hydrogen and carbon monoxide content of <math>\sim 70\%</math> (vol.) and <math>\sim 10\%</math> (vol.), respectively. The outcome shows that steam is a better gasifying agent for production of hydrogen rich syngas as compared to the (air + steam) gasifying mixture. The results also show that higher temperature favors hydrogen production however, a significant decrease in the HHV of the syngas was observed at elevated temperatures. Furthermore, the hydrogen conversion efficiency and energy conversion efficiency were calculated and were found to be 81 and <math>\sim 70\%</math>, respectively. Consequently, the</p>



	<p>produced syngas has the potential to be utilized as a renewable fuel in the industrial sector.</p> 
29.	<p><a href="#">Experimental investigation on hybrid turning of aluminum alloy using ultrasonic vibration and laser energy</a>  <b>N Deswal, R Kant - Machining Science and Technology, 2025</b></p> <p><b>Abstract:</b> Usage of cutting fluids during the machining of aluminum alloys enhances production costs and creates an unhealthy environment for nature and the operator. In the present work, ultrasonic vibration and laser energies are interacted with during the turning process simultaneously, and the process is termed ultrasonic-vibration-laser-assisted turning (UVLAT). Experiments are performed on aluminum alloy to compare the machinability among UVLAT, conventional turning (CT), ultrasonic vibration-assisted turning (UVAT) and laser-assisted turning (LAT). Outcomes revealed that low machining forces and low surface roughness are obtained for UVLAT compared with CT, UVAT and LAT. Diffusion and abrasive wear are observed during UVLAT, while adhesion and abrasive wear are observed during CT, UVAT and LAT. EDS analysis showed the adhesion of aluminum alloy on the tool face. Smooth edges, negligible chip segmentation and thin continuous chips are observed in UVLAT and UVAT, whereas thick continuous chips are observed in CT and LAT. The results showed that the machinability of aluminum alloys is enhanced in terms of reduced machining forces, lower tool wear, thin and negligible chip generation and lower surface roughness during UVLAT compared to the CT, UVAT and LAT processes.</p>
30.	<p><a href="#">Experimental investigation on metal, PM and unregulated emissions along with their toxicity from conventional diesel and RCCI engines employing gasoline and methanol as low reactivity fuels</a>  <b>NK Yadav, RK Maurya - Fuel, 2025</b></p> <p><b>Abstract:</b> Toxic metals and unregulated emissions from IC engines (ICEs), often overlooked in conventional regulatory frameworks, demand attention due to their potential health risks, even at trace levels. The present study conducts a comparative assessment of the toxicity of metal, unregulated, and particulate matter (PM) emissions from both conventional diesel (CDC) and gasoline/methanol-diesel (GD/MD) reactivity-controlled compression ignition (RCCI) engines. Instrumentation and modification are done to a single-cylinder automotive diesel engine to enable it to operate in RCCI mode, which involves integrating a port fuel injection system and installing pressure sensors. Gasoline and methanol are injected into the port during the intake stroke, and early direct injection of diesel is done to facilitate the transition to RCCI mode. The operational load of the engine and the premixed fuel ratio are systematically varied to investigate their effects on emissions and the associated toxicity levels. An in-vitro cytotoxicity assessment is performed using a human lung epithelial cell line (BEAS-2B) to evaluate the cytotoxic potential of PM emissions produced by both diesel and RCCI combustion modes. To evaluate the toxicity associated with metal and unregulated emissions, the potential inhalation cancer risk is assessed utilizing risk assessment formulations prescribed by regulatory bodies. Furthermore, the environmental risk associated with unregulated emissions is also assessed. The findings reveal that methanol-diesel RCCI shows promise in mitigating the cytotoxic effects of PM, particularly at medium load conditions, compared to both CDC and gasoline-diesel RCCI. Moreover, at lower engine loads, RCCI combustion exhibits a decrease in the cancer risk potential associated with metals compared to CDC combustion. Compared to CDC under medium load conditions, the RCCI combustion demonstrates a reduction in emissions equivalent to global warming,</p>

acidification, and eutrophication potentials. Despite its advantages, RCCI combustion engines exhibit higher levels of ozone-forming potential and cancer risk potential in their non-regulated emissions than CDC engines. However, as engine load increases, these potentials decrease in RCCI engines. Increasing the fuel premixing ratio under constant load conditions leads to a rise in both ozone-forming potential and cancer risk potential associated with non-unregulated emissions from RCCI engines.



### [Exploring improved hemodynamics in a stenosed artery using a two-phase Eulerian-granular blood model](#)

SS Das, C Sasmal - Physics of Fluids, 2025

31.

**Abstract:** Understanding the motion of red blood cells (RBCs) in stenosed blood vessels is critical for advancing knowledge of cardiovascular diseases such as atherosclerosis. This study employs a two-phase Eulerian-granular model to investigate hemodynamics in arteries with varying degrees of stenosis (DOS). By incorporating kinetic theory to account for RBC particle mechanics, the present model provides better predictive capabilities compared to single-phase Newtonian, non-Newtonian, and two-phase Euler–Euler models, showing better agreement with experimental data for straight arteries (0% DOS). The findings of this study reveal that stenosis significantly alters RBC distribution, deviating from the typical central plasma-surrounded configuration. The non-uniform RBC distribution in an artery significantly influences the corresponding velocity and vorticity fields, which again increases with the degree of stenosis. For instance, at 30% DOS, RBCs centralize more, while at 70% DOS, higher concentrations shift toward the proximal vessel wall. These changes again vary between the proximal and distal stenosed regions and across three different phases of the cardiac cycle, namely, acceleration (T1), peak systole (T2), and deacceleration (T3). Axial velocity profiles differ across the stenosed sections, with flow separation at 30% DOS and intensified recirculation at 70% DOS, both significantly influenced by cardiac phases. Turbulent kinetic energy (TKE) distribution is symmetric, peaking in T3 for 30% DOS and in T2 for 70% DOS. Area-averaged wall shear stress (AWSS) increases with DOS, particularly at the stenosis throat section. Furthermore, this study finds that the single-phase Newtonian model overpredicts flow separation and recirculation compared to the two-phase present approach. Overall, this study demonstrates the capability of the present two-phase model in capturing the impact of spatial RBC distribution on hemodynamics in stenosed arteries, offering potential extensions for the investigations of the hemodynamics of other complex biological systems.

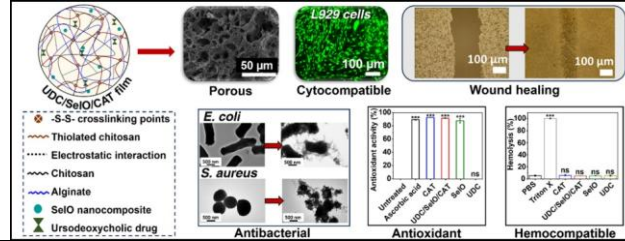
### [Fe/Se nanocomposite-loaded Chitosan/Alginate films for wound healing](#)

D Bhardwaj, V Chawla, A Gupta... Y Singh... - International Journal of Biological Macromolecules, 2025

32.

**Abstract:** Infectious wounds pose a major challenge to the healthcare sector, with numerous barriers, infections, dysregulated inflammation, and impaired cellular functions as well as complex healing mechanisms. To overcome these challenges, we report the fabrication of disulfide crosslinked chitosan/alginate (CAT)-based film loaded with iron oxide/selenium nanocomposite (SeIO) and ursodeoxycholic acid drug (UDC). Loading of SeIO and UDC in UDC/SeIO/CAT film leads to ~47 % increment in tensile strength as compared to CAT film. UDC/SeIO/CAT film shows the porosity of ~70 % and swelling ratios of around 800 % at physiological pH 7.4, which can aid in the enhanced drug release and efficient wound healing.

UDC/SeIO/CAT films exhibit a controlled degradation profile, and prolonged drug release of 92 % and 86 % at pH 7.4 and pH 8.5, respectively, over 110 h. It shows 99 % drug release at pH 5.5 over 74 h. Film displays 90 % antioxidant activity along with antibacterial activity of 86 % against *E. coli* and 89 % against *S. aureus*. Additionally, UDC/SeIO/CAT film is hemocompatible and exhibits good hemostatic behavior. It shows 130 % cell viability in murine fibroblast L929 cells, thus corroborating its cytocompatibility. Quantitative analysis of wound healing by scratch assay reveals 91 % decrease in wounded area on treatment with UDC/SeIO/CAT films.



### [Finding a promising CMOS inverter architecture with silicon nanosheet for future technology node](#)

**A Goel, A Rawat, B Rawat - IEEE Transactions on Electron Devices, 2025**

33.

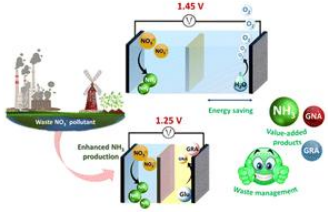
**Abstract:** In this work, we systematically explore the static and dynamic performance of silicon nanosheet (NSH)-based complementary metal-oxide–semiconductor (CMOS) inverters, including complementary field-effect transistor (CFET), forksheet (FSH), and standard stacked NSH (s-NSH) configurations, for the 5 nm and beyond technology node. The performance analysis of CMOS inverters is conducted using 3-D process simulations in fully calibrated technology computer-aided design (TCAD) simulation, which is based on the self-consistent solution of the Boltzmann transport equation and Poisson’s equation with quantum and mobility correction terms. Our findings reveal that the CFET inverter achieves remarkable advancements by offering around a 3.7% boost in operating frequency and around –3.7% reduction in power dissipation while decreasing the area footprint by approximately –60.8% compared with the s-NSH inverter for the 1-nm technology node. Although the FSH inverter slightly lags behind CFET in performance metrics, it still outperforms the s-NSH inverter by delivering an around 3% increment in the frequency at an equivalent power level and an area reduction of around –6.9%. Furthermore, CFET demonstrates superior resilience to process parameter variations, including doping fluctuation, oxide thickness, interface trap charges, and channel thickness. This robustness, combined with their compact design and excellent gate electrostatic control, enables CFET inverters to consistently outperform both FSH and s-NSH inverters across all evaluated technology nodes and design parameters. These advantages firmly establish the CFET inverter as the preferred choice for future ultrascale technology nodes and low-power logic applications.

### [Fluid dynamics of droplet impact and splitting on superhydrophobic wedges](#)

**GVVS Vara Prasad, P Kumar, P Dhar, D Samanta - Proceedings of the Royal Society A: Mathematical, Physical and Engineering Sciences, 2025**

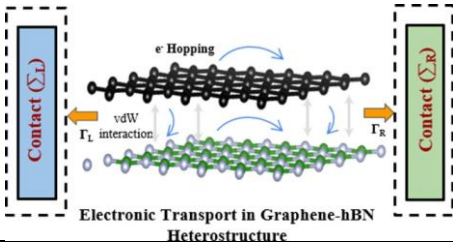
34.

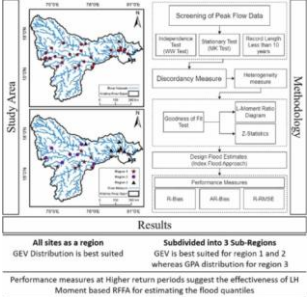
**Abstract:** We report an extensive computational and experimental investigation of droplet impact and subsequent splitting hydrodynamics on superhydrophobic wedges. Using two-dimensional (2D) and three-dimensional (3D) volume-of-fluid (VOF) simulations, supported by high-speed imaging experiments, we predict the impact, spreading, splitting, retraction and daughter droplet lift-off from superhydrophobic wedges. In particular, we examine how the wedge angle ( $\phi$ ), wedge asymmetry ( $\phi_1 - \phi_2$ ), Weber number ( $We$ ) and normalized Bond number ( $Bo^*$ ) influence the post-impact dynamics. We observe that for symmetric wedges, the maximum spread factor ( $\beta$ ) max of the droplet decreases with an increase in wedge angle ( $\phi$ ) at a fixed  $We$ . At high wedge angles, the sharp steepness of the wedge causes less contact area for the droplet to spread. For the asymmetric wedges, it has been noted that ( $\beta$ ) max increases with an

	<p>increase in <math>We</math> owing to the higher inertial forces of the droplet against sliding. Furthermore, <math>(\beta)</math> max increases with an increase in <math>Bo^*</math> at a fixed <math>We</math> owing to the dominance of the gravitational force over the capillary force of the droplet. It has also been found that at the same <math>Bo^*</math>, <math>(\beta)</math> max rises with an increase in <math>We</math> owing to the dominance of inertial forces over capillary forces. We discuss the non-dimensional split volume (<math>V^*</math>) of daughter droplets during the split-up stage for different symmetric and asymmetric wedge angles. In general, our 2D simulations agree well with the experiments for a major part of the droplet's lifetime. Further, we have conducted a detailed 3D simulation-based energy-budget analysis to estimate the temporal evolution of the various energy components at different post-impact hydrodynamic regimes.</p>
35.	<p><a href="#">High yield ammonia production via glucose oxidation assisted electrochemical nitrate reduction</a>  <b>A Chaturvedi, S Kaur, K Garg, TC Nagaiah - Journal of Materials Chemistry A, 2025</b></p> <p><b>Abstract:</b> The electrocatalytic nitrate (<math>NO_3^-</math>) reduction reaction (<math>NO_3RR</math>) provides a potential route for the synthesis of value-added ammonia (<math>NH_3</math>) and removal of nitrate pollutants. However, this reaction is limited by nitrate adsorption and slow kinetics involving multiple proton and electron transfer steps. The sluggish OER can hinder <math>NO_3RR</math> performance, but replacing it with a more facile oxidation process enhances performance. Herein, we have demonstrated the glucose oxidation assisted <math>NO_3RR</math>, utilizing <math>CuNi(1:2)S</math> as a bifunctional catalyst demonstrating a high <math>NH_3</math> faradaic efficiency (F.E.) of 93.44% with a yield rate of <math>4.7 \text{ mg h}^{-1} \text{ cm}^{-2}</math> or <math>280.47 \text{ mmol g}_{cat}^{-1} \text{ h}^{-1}</math> at <math>-0.4 \text{ V vs. RHE}</math> along with achieving high current densities of <math>\sim 118 \text{ mA cm}^{-2}</math> and its high activity compared to monometallic variants was explained using the ultraviolet photoelectron spectroscopy (UPS) technique. Furthermore, a mechanistic study using <i>in situ</i> electrochemical Raman spectroscopy, illustrates the hydrogenation of <math>NO_3^-</math> to <math>NH_3</math> via a <math>NO_2^-</math> intermediate. Moreover, replacing the OER with the glucose oxidation reaction (GOR) in a full cell system could decrease the total energy input by 200 mV and increase the <math>NH_3</math> yield from <math>120.95 \mu\text{g h}^{-1} \text{ cm}^{-2}</math> to <math>259.46 \mu\text{g h}^{-1} \text{ cm}^{-2}</math>. Furthermore, high value-added products were obtained at both the anode and cathode at a low cell voltage. More interestingly, we demonstrate the practical extraction of high-purity <math>NH_4Cl(s)</math> and <math>NH_3</math> aqueous products from electro-reduced <math>NO_3^-</math> after electrolysis at <math>100 \text{ mA cm}^{-2}</math> for 50 h, with a collection efficacy of 89.84% for the condensed <math>NH_3(aq)</math> solution.</p> 
36.	<p><a href="#">High-performance paper-based DNA-conjugated <math>Ti_3C_2T_x</math> bio-nanoelectrode for rapid point-of-care detection of HPV-16</a>  <b>R Rawat, S Singh, R Walia... - IEEE Sensors Journal, 2025</b></p> <p><b>Abstract:</b> Cervical cancer remains a significant global health concern, with High-Risk Human Papillomavirus (HR-HPV), particularly the genotype 16, identified as a key etiological factor with a significantly high mortality rate. The conventional diagnostic methods suffer from limitations related to efficiency and affordability, thereby necessitating the development of novel miniaturized biosensing platforms. In this study, we present the creation of an electroanalytical genosensor utilizing <math>Ti_3C_2T_x</math>/DNA hybrid screen-printed paper electrode strips for the detection of cervical cancer, based on varying concentrations of HPV-16. The Mxene nanostructures were characterized using X-Ray Diffraction (XRD), Field Emission Scanning Electron Microscopy (FESEM), Fourier Transform Infrared Spectroscopy (FTIR) and UV-Visible Spectroscopy (UV-Vis). While the performance of the bio-nanoelectrode towards HPV-16 detection was examined</p>



	<p>using Cyclic Voltammetry (CV) analysis. Meanwhile, the sensitivity and Detection limit (LoD) were calculated to be <math>1.65 \mu\text{A/fM/mm}^2</math> and <math>2.4 \text{ fM}</math> respectively, while being selective to HPV-16 DNA, as well as generating a shelf life of <math>\sim 1</math> month. The developed bio- nanoelectrode was further integrated with miniaturized electronics and 3D printing technology, while the resulting device – Cervicare demonstrating appreciable performance (<math>\text{LoD} = 0.02 \text{ pM}</math>). This indicates huge potential of the developed Cervicare device to be implemented within the point-of-care scenario, towards providing affordable healthcare among the affected populace.</p>
37.	<p><a href="#">Influence of ocean currents and surface tension on class II Bragg resonance using multi-scale analysis</a>  <b>D Goyal, TK Hota, SC Martha - Physics of Fluids, 2025</b></p> <p><b>Abstract:</b> This paper addresses how the ocean currents can influence the class II Bragg resonance of surface waves with non-zero surface tension interacting with bottom topography comprising of two different wavenumbers under the assumption of a small-amplitude wave theory. A multi-scale analysis technique is applied up to the third-order to obtain the analytical expressions for reflection and transmission coefficients by solving the coupled evolution equations involving the amplitudes of both reflected and transmitted waves. In the absence of current and surface tension, the findings are validated with the existing literature results. The Bragg peak decreases with increasing <math>U</math> and reaches closely to zero for <math>U</math> lying between <math>2.75</math> and <math>2.81 \text{ cm/s}</math> and further peak started to increase with increasing <math>U</math>. Phase shifting in the Bragg peak is observed in a non-monotonic manner with an increase in <math>U</math> as there is upshift when <math>U</math> changes from <math>0</math> to <math>2.75 \text{ cm/s}</math>, with sudden downshift at <math>U=2.77 \text{ cm/s}</math> and followed again by upshift for <math>U=2.81 \text{ cm/s}</math>. There is asymmetrical behavior in the amplitude of left and right subharmonic peaks that are observed for <math>U</math> lying between <math>2.75</math> and <math>2.81 \text{ cm/s}</math> and also, in the same range of <math>U</math>, the resonance bandwidth <math>B</math> is too short. These different qualitative behavior in the Bragg resonance is contingent upon the role played by the both positive and negative group velocities. The role of surface tension parameter <math>T</math> is also not trivial as the Bragg peak increases when <math>T</math> increases up to <math>U=2.81 \text{ cm/s}</math> but beyond this range, the effect of <math>T</math> is opposite which means the Bragg peak decreases when <math>T</math> increases. In addition to this, this study predicted that the choice of number of ripples <math>M</math> to achieve full reflection is dependent upon the value of <math>U</math>, and it is possible to accurately capture the effect of reflected energy for large values of <math>M</math>. Moreover, the subcritical detuning is observed in proximity to the Bragg resonance. This study has potential to build an understanding about the role of currents on higher-order Bragg resonance on the coastal bathymetries and extremely important for coastal rehabilitation.</p>
38.	<p><a href="#">Integrative deep learning framework for analysing population density shifts and flood inundation patterns</a>  <b>M Chaurasiya, S Chandra, S Kumar, S Sharma, A Kumar - Journal of Hydroinformatics, 2025</b></p> <p><b>Abstract:</b> This study introduces a robust deep learning framework to analyze the relationship between population density changes and flood inundation, which is crucial for improving disaster management and urban resilience strategies. As the environment changes, population grows rapidly, and infrastructure advances, it is vital to ensure urban areas can withstand floods while maintaining functionality and safety. Preparedness through anticipation and resource allocation in high-risk areas enhances risk assessment. Using high-resolution satellite imagery, socio-economic datasets, and a modified U-Net architecture to process multispectral and Synthetic Aperture Radar (SAR) data, the study generates detailed maps of population shifts and flood extents. The Intersection over Union (IoU) metric rigorously validates the model's accuracy in predicting and mapping flood and population data. The findings show significant correlations between flood events and population distribution changes, offering empirical insights into infrastructure development and resilience planning. These insights help develop effective policies to manage urbanization and population in flood-prone areas. Additionally, the results provide data-driven insights for infrastructure and resilience planning in response to climate change</p>

	<p>challenges. This information aids policymakers in addressing the impacts of climate change on vulnerable communities, supporting community empowerment, and facilitating early restoration post crisis.</p>
39.	<p><a href="#">Interfacial configuration-driven transport properties in graphene-hBN heterostructures</a>  <b>Renu, K Katin, S Chakraborti... R Kumar</b> - The Journal of Physical Chemistry C, 2025</p> <p><b>Abstract:</b> Transport properties of heterostructures differ from those of the constituent two-dimensional materials due to van der Waals (vdW) interactions and the strength of the interlayer coupling. In this work, we investigated the effect of interfacial configurations on vdW interactions and the electronic transport properties of graphene-hBN heterostructures using density functional theory (DFT) and a tight-binding approximation. The surface charges are redistributed in the heterostructures depending on the strength of the vdW interactions that drive interfacial configurations. It is noted that the interfacial configuration with the maximum charge redistribution has the maximum inter- and intralayer electronic transport characteristics. As a consequence, the transport properties are found to be strongly dependent on the interfacial configuration of the heterostructures. The results provide valuable insights into interfacial configurations in designing heterostructures from 2D materials for electronic devices based on the transport properties such as transistors and sensors.</p> 
40.	<p><a href="#">LH-moment-based regional flood frequency analysis framework to determine design floods in Krishna River basin</a>  <b>AK Singh, SR Chavan</b> - Journal of Hydrology: Regional Studies, 2025</p> <p><b>Abstract:</b> Study region: Krishna River basin, India Study focus: There have been limited efforts to develop the LH-moment-based Regional Flood Frequency Analysis (RFFA) framework for Indian catchments. In this study, the LH-moment-based RFFA is used to determine flood quantiles at ungauged sites within the Krishna River basin in India, corresponding to various return periods. Three probability distributions, namely the generalized extreme value (GEV), generalized logistic (GLO), and generalized Pareto (GPA) are considered for performing the RFFA. New hydrological insights for the region: This study examines two cases for RFFA, viz., the first involves a single region comprising all 24 gauges within the basin, while the second divides the 24 gauges into three hydrologically similar regions based on the global K-means (GKM) clustering algorithm. The discordancy and heterogeneity measures are considered for the screening of the peak flow data and checking the heterogeneity of the formed regions, respectively. The performance of the LH-moment-based RFFA framework is evaluated through the Leave-One-Out Cross-Validation (LOOCV) experiment. In the case of single region, GEV distribution is found to be the most suitable regional distribution, while in the second case, the GEV{GEV}[GPA] is identified as the best-fitted regional distribution for the region 1{2}[3]. Overall, the study demonstrates the efficacy of the higher-order LH-moment-based RFFA framework over the L-moment.</p>

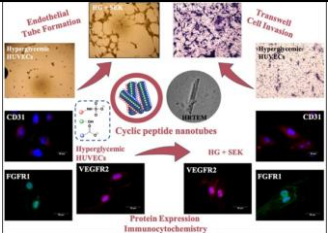
	 <p>The figure consists of two maps of a study area and a flowchart. The top map shows the study area with various sites marked. The bottom map shows the study area with various sites marked. The flowchart details the process from peak flow data screening to final results, including sub-region analysis and performance measures.</p>
41.	<p><a href="#">Mathematical modelling and simulation of machine calender used in electrode production for running electric vehicles</a>  <b>S Rangra, N Kanth, J Kumar</b> - Journal of The Electrochemical Society, 2025</p> <p><b>Abstract:</b> Due to the continuous increase in demand for electric vehicles which run on lithium-ion batteries, the need to improve their performance is also increasing. As a result, optimizing each manufacturing stage is critical, out of which calendaring is a final stage of electrode production in which electrodes are compressed while passing through a stack of hard/soft bowls, leading to changes in the electrode's porosity, thickness, density, smoothness, adhesion/bonding strength, wettability, and coating homogeneity. Calendered electrodes enhance volumetric energy density, rate capability, cyclic rate, and life span of the batteries. Hard/soft bowls used in a calendaring machine have a covering/layering of either chilled cast iron or fragile material (nylon, cotton, or rubber) with varying thickness. Here we report on an investigation of the influence of cover thickness along with other design and process parameters of machine calender namely bowl diameter, bulk modulus and line load on the contact width with the help of a generalized nip mechanics model. Additionally, the influence of bowl temperature and contact time on the electrode sheet was investigated with the help of heat transfer model.</p>
42.	<p><a href="#">Memory optimal distance-2-dispersion with termination</a>  <b>T Kaur, K Mondal</b> - International Journal of Parallel, Emergent and Distributed Systems, 2025</p> <p><b>Abstract:</b> The aim of the dispersion problem is to place a set of <math>k</math> (<math>k \leq n</math>) mobile robots in the nodes of an unknown graph consisting of <math>n</math> nodes such that in the final configuration each node contains at most one robot, starting from any arbitrary initial configuration of the robots on the graph. In this work, we propose a variant of the dispersion problem, namely Distance-2-Dispersion, in short, D-2-D, where we start with any number of robots, and put an additional constraint that no two adjacent nodes contain robots in the final configuration. That is, the distance between any two nodes with robots must be at least 2. However, even if the number of robots <math>k</math> is less than <math>n</math>, it might be the case that it is not possible for each robot to find a distinct node to reside, maintaining our added constraint. More specifically, if a maximal independent set is already formed by the nodes containing a robot each, then any other unsettled robot will not find a node to settle. Hence we allow multiple robots to sit on some nodes only if there is no place to sit. If <math>k \geq n</math>, it is guaranteed that the nodes with robots form a maximal independent set of the underlying network. The graph <math>G=(V,E)</math> is a port-labeled graph with <math>n</math> nodes and <math>m</math> edges, where nodes are anonymous. The robots have unique IDs in the range <math>[1, L]</math>, where <math>L \geq k</math>. Co-located robots can communicate among themselves. We provide an algorithm that solves D-2-D starting from a rooted configuration (i.e. initially all the robots are co-located) and terminates after <math>2 \times \Delta \times (8 \times m - 3 \times n + 3)</math> synchronous rounds using <math>O(\log n)</math> memory per robot, without using any global knowledge of the graph parameters <math>m, n</math> and <math>\Delta</math>, the maximum degree of the graph. We provide <math>\Omega(\log n)</math> lower bound on the memory requirement by the robots to solve the D-2-D problem. Thus our algorithm is memory-optimal. We conjecture that the time required by the robots to solve the D-2-D problem, provided each of them have <math>O(\log n)</math> memory, is <math>\Omega(m \times \Delta)</math> rounds. We further show that if the nodes are also equipped with a storage of <math>O(\log n)</math> bits, then even if the robots are arbitrarily positioned at the nodes of the graph in</p>

	<p>the initial configuration, they can solve the problem of D-2-D in <math>2 \times \Delta \times (8 \times m - 3 \times n + 3) + 8 \times m</math> rounds in the same setting.</p> <ul style="list-style-type: none"> <li>• We introduce a new problem by adding an extra constraint on the problem of dispersion, which is a well-studied problem in the area of mobile computing. We name this problem as Distance-2-Dispersion (D-2-D). With <i>enough</i> robots, this problem becomes equivalent to finding a maximal independent set.</li> <li>• We provide an algorithm that solves D-2-D from a rooted initial configuration and terminates in <math>O(m\Delta)</math> rounds, provided each robot has <math>O(\log n)</math> memory. Here, <math>\Delta</math> denotes the maximum degree of the graph, <math>m</math> and <math>n</math> are the number of edges and the number of nodes in the graph, respectively. The robots do not require any prior knowledge of any of the global parameters.</li> <li>• We provide an <math>\Omega(\log n)</math> lower bound on the memory requirement per robot to solve the problem of D-2-D. We also conjecture that the robots require <math>\Omega(m\Delta)</math> time to solve D-2-D provided they have <math>O(\log n)</math> memory.</li> <li>• We further show that if the nodes also have additional storage of <math>O(\log n)</math> bits, then the robots can solve the problem of D-2-D in <math>O(m\Delta)</math> rounds in the same setting starting from an arbitrary initial configuration.</li> </ul>
43.	<p><a href="#">Multiview attention fusion for explainable body language behavior recognition</a>  <b>S Madan, R Jain, R Subramanian, A Dhall</b> – IEEE Transactions on Affective Computing, 2025</p> <p><b>Abstract:</b> Body language behavior, including gestures and fine-grained movements not only reflects human emotions, but also serves as a versatile cue for enhancing emotional intelligence and creating responsive technologies. In this work, we explore the efficacy of multiview-multimodal cues for explainable prediction of bodily behavior. This paper proposes an attention fusion method that combines features extracted from (1) multiview videos termed “RGB”, (2) their multiview Discrete Cosine Transform representations termed “DCT” and (3) three stream skeleton features termed “Skeleton”, via a transformer-based approach. We evaluate our approach on the diverse BBSI [1] and Drive&amp;Act [2] datasets. Empirical results confirm that the RGB, DCT and Skeleton features enable discovery of multiple class-specific behaviors resulting in explainable predictions. Our key findings are: (a) Multimodal approaches outperform unimodal counterparts in categorizing bodily behavioral classes; (b) Efficient class predictions and plausible explanations are achieved with both unimodal and multimodal approaches; and (c) Empirical results confirm the superiority of our approach compared to state-of-the-art methods on both datasets. Our implementation code is available at: <a href="https://github.com/surbhimadan92/MAGIC_TBR_Extended">https://github.com/surbhimadan92/MAGIC_TBR_Extended</a>.</p>
44.	<p><a href="#">Natural Gas and hydrogen blending: A perspective on numerical modeling and CFD analysis for transient and steady-state scenarios</a>  <b>S Sharma, AH Sahir</b> - Chemical Product and Process Modeling, 2025</p> <p><b>Abstract:</b> The integration of hydrogen as an energy carrier into an existing natural gas pipeline infrastructure presents a promising option for the decarbonization of the energy sector. However, using hydrogen in natural gas pipelines requires overcoming engineering challenges attributed to physical property and design considerations for both natural gas and hydrogen which may result in pipeline failures. To this end, this study employs a multi-software engineering approach to model both steady-state and transient behaviors of natural gas pipelines blended with hydrogen under cyclic variations. For transient state modeling, the Crank-Nicolson implicit scheme is applied to a 100 km pipeline with 200 nodes, using a time interval of 20 s in MATLAB. The one dimensional flow modeling aspects are analyzed in more detail with the finite element method in COMSOL. The study also highlights the importance of pipeline inventory analysis, focusing on the trade-off between gas transport capacity and flexibility; particularly with respect to packing and drafting operations. The intrinsic properties of hydrogen blends (0–20 %) are analyzed using the GERG Equation of State (EoS) in ASPEN. Results indicate that the COMSOL model shows less stability than the Crank-Nicolson method for abrupt demand changes, with a percentage error of <math>\pm 11\%</math> compared to the benchmark study. Additionally, inventory analysis suggests that to prevent pipeline failure, the pipeline can only be drafted for 3.6 h. Steady-state analysis reveals that blending hydrogen into natural gas significantly impacts pipeline design, with changes in specific gravity, compressibility factor, and speed of sound. The study also finds that higher hydrogen blending reduces the pressure drop under isothermal conditions, resulting in lower</p>



	compressor power requirements. This modeling approach provides a foundation for strategies aimed at adapting natural gas infrastructure for hydrogen use.
45.	<p><a href="#">Numerical study of a hybrid battery thermal management system for enhanced thermal regulation in electric vehicles</a>  <b>D Yogeshwar, R Repaka, R Nadda - Journal of Thermal Analysis and Calorimetry, 2025</b></p> <p><b>Abstract:</b> This study numerically investigates the thermal performance of a three-dimensional battery thermal management system (BTMS) incorporating a rectangular cooling plate with a serpentine channel. The current study mainly focuses on cooling the positive and negative terminals of batteries in a module using air and liquid cooling strategies under varying discharge rates (0.7C, 1C, and 1.5C), cooling plate configurations, and fluid velocities. A Newman P2D electrochemical–thermal model is employed to simulate thermal energy generation and is coupled with fluid flow and heat transfer models to ensure mass, momentum, and energy conservation. The results indicate that increasing air velocity to <math>5 \text{ ms}^{-1}</math> in air-cooled BTMS reduces <math>T_{\text{max}}</math> by 9.75 K, 10.21 K, and 9.73 K for 0.7C, 1C, and 1.5C discharge rates, respectively, with minimal reduction beyond this velocity, establishing <math>5 \text{ ms}^{-1}</math> as optimal. Further, incorporating two cooling plates reduces <math>T_{\text{max}}</math> to 304.42 K and <math>\Delta T</math> to 3.15 K at 0.7C, while three cooling plates achieve <math>T_{\text{max}}</math> of 305.40 K and <math>\Delta T</math> of 3.89 K at 1C, demonstrating optimal designs for this discharge rates. At 1.5C discharge rate, the hybrid BTMS with three cooling plates, with a water velocity of <math>0.10 \text{ ms}^{-1}</math>, lowers <math>T_{\text{max}}</math> to 305.69 K and <math>\Delta T</math> to 4.43 K, achieving optimal cooling. Compared to air-cooled BTMS, hybrid BTMS with a rectangular cooling plate reduces <math>T_{\text{max}}</math> by 7.03%, 8.73%, and 11.41% for 0.7C, 1C, and 1.5C, respectively, maintaining battery temperatures below operating limit (308.15 K) with <math>\Delta T &lt; 5 \text{ K}</math>, ensuring thermal uniformity.</p>
46.	<p><a href="#">Oblique water wave scattering by a step</a>  <b>D Goyal, SC Martha, BN Mandal - Journal of Engineering Mathematics, 2025</b></p> <p><b>Abstract:</b> The article is concerned with oblique scattering by a step, infinite or finite. The waves can be obliquely incident from either higher depth region to lower depth region or lower depth region to higher depth region in both the cases. The problem is formulated in terms of solving first-kind integral equation on the unknown horizontal component of velocity above the step. The unknown is approximated via multi-term Galerkin technique in terms of product of simple polynomials and exponential decay function multiplied by a suitable weight functions whose form is determined by the edge condition at the step's corner. This reduces the integral equation to a system of linear equations which are solved numerically. Reflection and transmission coefficients are computed using the numerical solution of the integral equation. The numerical results are validated by comparing with known results available in the literature. It is found that increasing the angle of incidence increases the reflection of the wave incident from either direction for both positions of step. The critical values of depth ratios are also observed corresponding to angle of incidence and frequencies for finite step for which maximum reflection occurs. Additionally, for lower frequencies which are less than or equals to <math>10^{-1}</math>, there occurs critical angle of incidence for which reflection is minimum for both positions of step. This study will provide enough information about the wave behavior in the oceanic areas where these step kind of bottoms are present and is helpful for the ocean engineers before building any infrastructure in these regions.</p>
47.	<p><a href="#">Optimal control and homogenization of semi-linear parabolic problem with highly oscillatory coefficients in an oscillating domain</a>  <b>AK Nandakumaran, R Raj, BC Sardar - Nonlinear Differential Equations and Applications NoDEA, 2025</b></p> <p><b>Abstract:</b> In this article, we explore the homogenization of an optimal control problem driven by a semi-linear parabolic equation within a two-dimensional oscillating domain, denoted as <math>\Omega_\epsilon</math>. The state equation and cost function in this scenario involve periodic coefficients, <math>A_\epsilon</math> and <math>B_\epsilon</math>,</p>

	<p>which exhibit significant oscillations. The objective of this study is to analyze the limiting behavior of both the optimal control and the corresponding state as the oscillations become increasingly fine. Furthermore, we aim to identify the optimal control problem that encapsulates the effects of these oscillating coefficients and to establish a corrector result for the state variable.</p>
48.	<p><a href="#">Philosophy of health in ancient Indian martial art: Traditional knowledge of <i>marma</i> embedded in <i>kalaripayattu</i> and the health benefits of its practice</a>  <b>A Nandha, A V Suresh</b> - Indian Journal of History of Science, 2025</p> <p><b>Abstract:</b> This paper expounds on the philosophy of health in the Indian martial art form of <i>kalaripayattu</i> by detailing the traditional knowledge of the concept of <i>marma</i> rooted in the martial art form and demonstrating the health benefits of practicing <i>kalaripayattu</i> using a qualitative study. This paper argues that this martial art conceptualized with knowledge of human body enhances the health benefits of practitioners of <i>kalaripayattu</i>. It is part of the cultural fabric of the southwestern Indian state, Kerala. Proudly showcased in posters of Kerala's tourism and cultural promotional activities, this martial art occupies more than just physical activity status. Historically, <i>kalaripayattu</i> was part of the judicial system of the present-day regions of Kerala, and its practitioners were highly regarded in the social hierarchy. They prescribed ways of healthy living, and these habits were entrenched in the local culture. The present study aims to understand the philosophy behind ancient Indian health practices with the objective of reviving this martial art. The article explores concepts of <i>marma</i> (seats of vitality) as the underlying principle of understanding human anatomy. <i>Kalaripayattu</i> employs the knowledge of <i>marma</i> points to revitalize or debilitate people. This article also details the findings of a qualitative study regarding the health benefits of practicing <i>kalaripayattu</i>.</p>
49.	<p><a href="#">Proangiogenic cyclic peptide nanotubes for diabetic wound healing</a>  <b>V Chawla, S Roy, J Raju, P Bundel, D Pal, Y Singh</b> - ACS Applied Bio Materials, 2025</p> <p><b>Abstract:</b> An intricate biochemical system of coordinated cellular reactions is involved in restoring damaged tissue after wounds. In chronic wounds, such as diabetic foot ulcers, poor angiogenesis is a common stumbling block due to elevated glucose levels, increased proteolytic enzyme activity, and decreased production of growth factors. While various strategies, including modulation of inflammatory cells, administration of growth factors, and therapies involving stem cells or genes, have been explored to promote angiogenesis, they often suffer from limitations such as poor biodistribution, immunological rejection, administration/dosing, and proteolytic instability. Glycosaminoglycans, such as heparan sulfate, facilitate growth factor interactions with their receptors to induce angiogenic signaling, but their exogenous administration is hindered by poor stability, low serum half-life, and immunogenicity. Cyclic peptides, known for their structural stability and specificity, offer a promising alternative for inducing angiogenesis upon functional modifications. In this work, we developed heparan sulfate (HS)-mimetic cyclic peptide nanotubes (CPNTs) grafted with bioactive groups to enhance angiogenesis without using exogenous growth factors, drugs, or supplements. These CPNTs incorporate glutamic acid, serine, and sulfonated lysine to mimic the functional groups in heparin. The sulfonated cyclic hexapeptide nanotubes developed from <sup>D</sup>Pro-<sup>L</sup>Trp-<sup>D</sup>Leu-<sup>L</sup>Ser-<sup>D</sup>Glu-<sup>L</sup>Lys demonstrated significant proangiogenic activity in HUVECs under hyperglycemic conditions; enhanced endothelial cell motility, invasion, and tube formation; and upregulation of proangiogenic genes and proteins. These HS-mimicking nanotubes have shown a strong potential for promoting impaired angiogenesis, without incorporating exogenous growth factors, and show strong potential in treating diabetic wounds. To the best of our knowledge, this is the first report on the use of HS-mimetic proangiogenic cyclic peptide nanotubes for diabetic wound healing.</p>

			
50.	<a href="#">Recent advances in synthesis and photophysical applications of pyridine-based heterocycles</a> DR Mishra, DK Sahoo, NP Mishra - Asian Journal of Organic Chemistry, 2025	<p><b>Abstract:</b> Pyridine-based heterocyclic compounds have seen significant advancements in their synthesis and photophysical applications. Researchers have pioneered innovative synthetic methods that enhance the efficiency and versatility of these compounds, leading to notable improvements in their photophysical properties. Consequently, pyridine-based fluorophores are now being utilized across various fields, including bioimaging, sensing, and photonic devices. Their distinctive characteristics as tuneable emission wavelengths and enhanced stability make them well-suited for numerous applications, ranging from tracking biomolecules in living cells to improving the performance of optoelectronic systems. This review underscores the emerging potential of pyridine-based compounds in both scientific research and industrial applications, setting the stage for future innovations.</p>	
51.	<a href="#">SmartDeCoup: Decoupling the STT-RAM LLC for even write distribution and lifetime improvement</a> P Sinha, KP BV, S Das, VK Tavva - Journal of Systems Architecture, 2025	<p><b>Abstract:</b> Static Random Access Memory (SRAM) based Last Level Caches (LLCs) is losing its edge to Non-Volatile Memories (NVMs) like Spin-Transfer Torque RAM (STT-RAM) which offer advantages including higher density and lower static power consumption. However, they have drawbacks, namely, higher write latency, higher write power consumption, and lower write endurance. Uneven distribution of writes leads to reduced write endurance. Existing endurance enhancement techniques focus on reducing write variation to extend the lifetime. Additionally, these techniques cannot be implemented on top of recent secure cache designs that protect LLCs from timing channel attacks. They cannot prevent recently proposed endurance attacks on the STT-RAM LLC. SmartDeCoup proposes a decoupled tag/data array structure for STT-RAM LLCs and, on top of this structure, introduces two approaches to enhance LLC lifetime through: (a) the Primal Approach, and (b) the Hardware Efficient Approach. The Primal Approach achieves a maximum relative lifetime improvement of 24.99× and 33.13× in single core and multicore systems, with a 8.79% area overhead. The Hardware Efficient Approach achieves improvements of 22.47× and 31.83×, with a 7.23% area overhead. The Primal Approach is capable of preventing endurance attacks and is also compatible with the recently proposed countermeasures for timing channel attacks on LLC.</p>	
52.	<a href="#">Synergizing machine learning and fluorescent biomolecules: A new era in sensing platforms</a> N Saini, A Thakur...N Singh - TrAC Trends in Analytical Chemistry, 2025	<p><b>Abstract:</b> Machine Learning (ML) algorithms offer significant advantages over traditional methods, enabling the identification of complex correlations and hidden patterns within data, which enhances efficiency, reduces costs, and improves decision-making. This article provides a comprehensive overview of recent advances in ML-assisted fluorescent peptide and protein-based sensors. Notably, a supervised ML-assisted peptide-based sensor has been developed for the identification of water-soluble polymers, improving environmental and industrial monitoring. ML-assisted sulfonamido-oxine (SOX)-labeled peptides facilitate the quantitation of mitogen-activated protein kinases, advancing sensitive biomarker analysis. An array-based detection system using green fluorescent protein conjugates enables high-throughput protein screening. A</p>	

deep learning (DL)-assisted fluorophore-labeled peptide sensor array shows promise for non-invasive breast cancer diagnosis with high accuracy. Additionally, a ML-aided sensor array combining antimicrobial peptides and fluorescent proteins enables the discrimination of top clinical isolates, enhancing antimicrobial resistance diagnostics. These innovations in peptide sensor design and ML integration highlight their transformative impact in biological research, disease diagnostics, and environmental monitoring, offering improved sensitivity, selectivity, and performance. This review provides valuable insights for researchers and practitioners in the field of fluorescence-based sensing, ML, and their interdisciplinary applications.



[Tailored fibrils approach via Ag\(I\).peptidomimetic-based interface design: Efficient encapsulation of diverse active pharmaceutical ingredients in wastewater remediation during effluent treatment plant \(ETP\) processing](#)

**A Sharma, N Kaur, N Singh - Langmuir, 2025**

53.

**Abstract:** Pharmaceutical pollution in wastewater poses significant environmental and public health concerns worldwide. Chloramphenicol (CP), an antibiotic widely used in medical and veterinary applications, is among the active pharmaceutical ingredients (APIs) frequently detected in aquatic environments. This study explored the encapsulation of chloramphenicol API in contaminated wastewater using rationally designed fibrillations based on the silver metal ion-directed self-assembly of fibrillator-type self-assembling ligand (**ANS-3**). We further investigated the removal of various commonly prescribed drugs, including antibiotics such as  $\beta$ -lactam (amoxicillin), fluoroquinolone (ciprofloxacin), aminoglycoside (neomycin), and tetracycline; antiparasitic agents with antiprotozoal properties (praziquantel and metronidazole); nonsteroidal anti-inflammatory drugs (NSAIDs) such as phenylbutazone and ketoprofen; the vasodilator isoxsuprine; amphiphilic antidepressants (amitriptyline); and the antiviral drug amantadine. The findings validated the crucial influence of polar multifunctionality and structural complexity in enhancing interactions with **Ag.ANS-3** matrix, emphasizing its potential for efficient drug sequestration. First, picolinic acid (PA) and phenylalanine (F) were evaluated for their ability to form fibrillar structures, and their morphological characterization revealed well-defined fibrillar networks with varying degrees of porosity and interconnectivity. Then, the strategic inclusion of leucine in synthesizing **ANS-3** facilitated the formation of robust fibrillar networks, employing its hydrophobic interactions to drive the self-assembly process. Finally, the encapsulation of APIs was evaluated using Ag(I) metal ion-driven **ANS-3** based self-assembled nanofibrous material. This research contributes to the development of innovative physicochemical wastewater treatment strategies for environmental remediation and validates the importance of rational design in encapsulation-based wastewater remediation technologies.



54.

[The scattering of water waves by M-floating porous plates over  \$\(M - 1\)\$ -trenches](#)

**S Choudhary, SC Martha, T Sahoo - Journal of Offshore Mechanics and Arctic Engineering, 2025**

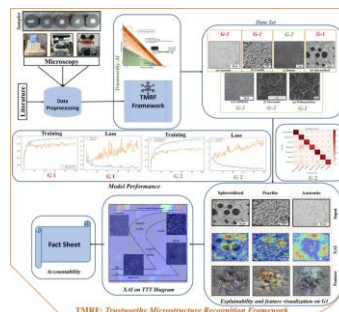


**Abstract:** This paper investigates the interaction of water waves with multiple thin horizontal floating porous plates over multiple trenches at the bottom. The boundary value problem is solved for velocity potential using Havelock's expansion and algebraic least-square method. To understand the advantage of multiple porous plates and trenches, the numerical results are plotted for the scattering and dissipation coefficients through different graphs to examine the effect of various parameters. In the direction of the use of a minimal number of porous plates in the absence of trenches, it is observed that the curves almost coincide for the three and four-plate cases, implying three plates will be sufficient for maximum wave energy dissipation and minimal wave transmission. But, for the case of two trenches and in the absence of porous plates, the curves show an oscillatory pattern with harmonic and sub-harmonic peaks. The study also shows that the oscillating pattern in the curves vanishes when there are two trenches and three porous plates with moderate values of the porous effect parameter. In the latter case, plates with larger lengths will produce almost zero transmission and dissipate or reflect a major part of the incident wave energy. It is concluded that the above-specific combination of barriers and plates dissipates maximum wave energy and transmits a very small amount, providing a safer zone in the trench regions. Thus, multiple navigation channels can be created to overcome the issues of dense vessel traffic arising in a single channel.

[TMRF: Trustworthy microstructure recognition framework with deep learning and explainable AI](#)

[A Pratap, PA Hsiung, N Sardana - Journal of Materials Research, 2025](#)

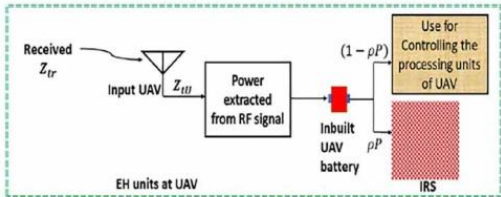
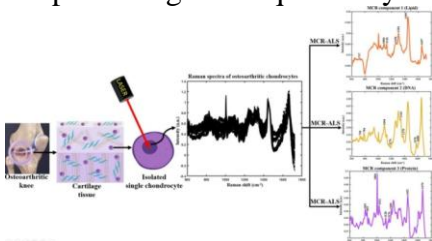
**Abstract:** This study introduces the Trustworthy Microstructural Recognition Framework (TMRF), aimed at enhancing microstructural recognition with a focus on explainability, human-computer interaction, and accountability. Evaluating microstructural images across seven classes, the framework employed transfer learning models in two experiments: Group 1 (three distinct classes) and Group 2 (all classes). DenseNet outperformed other models, achieving 97% accuracy and 96% F1 scores. Explainable AI (XAI) improved interpretability, with Occlusion and SmoothGrad providing insertion fidelity scores of 60% and 50% for Group 1 and Group 2, respectively. Visualization highlighted the model's detailed understanding of Group 1's microstructures. Practical demonstration over the Time-Temperature-Transformation (TTT) diagram showcased Group 1's impeccable micrograph identification. The TMRF Fact Sheet, emphasizing explainability, underscores the framework's role in fostering trust in microstructural recognition systems.



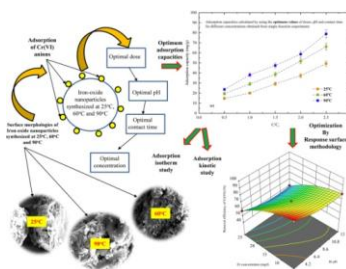
[UAV-assisted irs system with energy harvesting: Enhanced reliability in critical scenarios for 5G/6G wireless communication](#)

[P Kumar, S Kamath, S Darshi, JY Pan, M Iqbal, S Shailendra, V Mohan - IEEE Access, 2025](#)

**Abstract:** This paper proposes an UAV-assisted intelligent reflecting surface (IRS) system for improving the network performance between ground-to-ground (G2G) users in 5G/6G wireless communication. This work may be applicable for packet delivery in bustling urban areas, especially where G2G links are in deep fade. For energizing the IRS elements and controlling the processing units of the UAV, radio-frequency (RF)-based energy harvesting (EH) is proposed at

	<p>UAV, where the dynamic power splitting factor depends on the height-dependent Nakagami-m shaping parameter (<math>m</math>). The mathematical framework for the proposal includes the height-dependent Nakagami-m fading to represent small-scale fading and height-dependent path-loss exponent to model large-scale fading. We develop the expression for spectral efficiency and derive a closed-form expression of an outage probability for the proposed scenario by considering Nakagami-m channel among A2G links. The analytical results are validated with simulation results, and the work is compared with the existing state-of-the-art.</p> 
57.	<p><a href="#">Unravelling changes in single-cell osteoarthritic chondrocytes through coupling of Raman spectroscopy and multivariate curve resolution-alternating least square (MCR-ALS) algorithm</a>  <b>G Uppal, T Goyal, A Kumar, R Kumar - Microchemical Journal, 2025</b></p> <p><b>Abstract:</b> Chondrocyte apoptosis is one of the major factors in degeneration of articular cartilage in osteoarthritis (OA). A comprehensive understanding of the biochemical changes at the molecular level during apoptosis is essential for elucidating the complex mechanisms underlying cartilage degeneration in OA. Raman spectroscopy (RS) could be a robust tool for revealing biochemical changes occurring at the single-cell level, as it enables to uncover the early-stage changes and the identification of multiple molecular components without the need for external labeling, all under physiological conditions with minimal or no sample processing. However, one of the major challenges associated with Raman analysis of biological samples is the overlap of spectral peaks arising from various molecular components, which can complicate the interpretation of spectral data. In this work, multivariate curve resolution – alternating least squares (MCR-ALS) was applied to deconvolve the Raman spectra acquired from the nucleus of chondrocytes extracted from osteoarthritic human knee articular cartilage (grade-I, II, and III). The MCR-ALS analysis identified spectral components corresponding to lipids, DNA, and proteins, and showed that the concentration of DNA and proteins decreased, while lipid content increased in chondrocytes with the progression of osteoarthritic degeneration in articular cartilage. The findings using the combination of Raman-MCR, along with statistical analyses of Raman spectral peaks and further examination of the amide-I bands, provided valuable insights into the biochemical changes in apoptotic chondrocytes during OA progression. The study demonstrated that the combination of Raman-MCR has the potential to be used for the deconvolution of composite Raman spectra and determine label-free spectral markers for single-cell molecular analysis, making it a promising technique for cytodiagnosis.</p> 
58.	<p><a href="#">Using iron-oxide nanoparticles synthesized at varying temperatures to remove Cr(VI): Characterization, adsorption mechanism, and optimization study</a>  <b>S Ganguly, S Ganguly - Surfaces and Interfaces, 2025</b></p> <p><b>Abstract:</b> Hexavalent Chromium [Cr(VI)] is a toxic heavy metal and a notable health hazard. Thus, proper remediation method must be employed for its removal from contaminated water. Iron-oxide nanoparticles have been employed multiple times as an adsorbent for the removal of</p>

Cr(VI); however, the adsorption capacity obtained was not sufficiently high. Therefore, this study attempts to synthesize iron–oxide nanoparticles at different temperatures of 25 °C, 60 °C, and 90 °C, respectively and improve both its adsorption efficiency and capacity substantially. Firstly, the iron–oxide nanoparticles were synthesized by the co–precipitation method and investigations on the surface morphologies, sizes, chemical compositions and magnetic properties were carried out by several characterization methods. Next, iron–oxide nanoparticles were used as adsorbents in batch equilibrium studies to effectively remove Cr(VI). A number of parameters, including dosage and contact time, were examined in order to determine how they affected the adsorption process. Using the iron–oxide nanoparticles synthesised at 25 °C (room temperature), 60 °C, and 90 °C, the optimal removal efficiencies recorded were 81.78%, 82.29%, and 83.82% for a Cr(VI) content of 10 mg/L, respectively. Subsequent optimization experiments were conducted with the Box–Behnken Design approach (BBD) in order to emphasise the interactions among the parameters. The adsorption efficiency was used as the response variable in the development of a 2<sup>nd</sup>–order quadratic equation, and the proposed model's feasibility was assessed using an ANOVA test. Several adsorption isotherm and kinetic models were analysed and the most appropriate model to define the adsorption mechanism and the rate-limiting steps were determined.



**Disclaimer:** This publication digest may not contain all the papers published. Library has compiled the publication data as per the alerts received from Scopus and Google Scholar for the affiliation “Indian Institute of Technology Ropar” for the month of March, 2025. The author(s) are requested to share their missing paper(s) details if any, for the inclusion in the next publication digest.